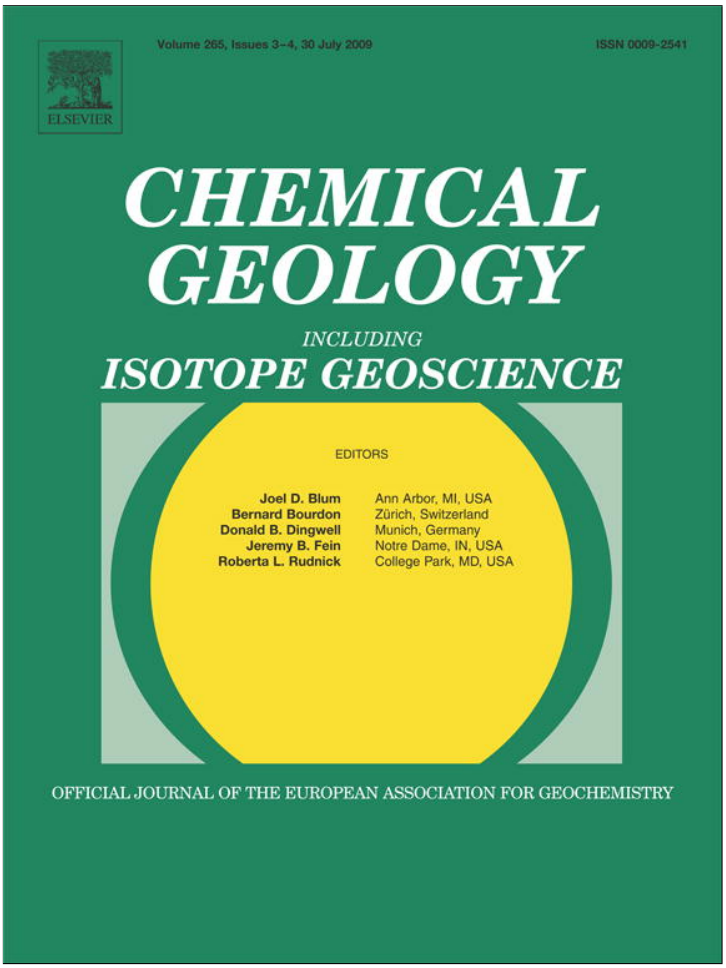

Chemical Geology 265 (2009) 335–344

Contents lists available at ScienceDirect

Chemical Geology

journal homepage: www.elsevier.com/locate/chemgeo

$CaCl_2$-hydrate nucleation in synthetic fluid inclusions

Miriam Baumgartner, Ronald J. Bakker *

Department of Applied Geosciences and Geophysics, Mineralogy and Petrology, University of Leoben, Leoben, Austria

ARTICLE INFO

Article history:
Received 23 February 2009
Received in revised form 21 April 2009
Accepted 22 April 2009

Editor: J. Fein

Keywords:
$CaCl_2$-hydrates
Metastability
Fluid inclusions
Raman spectroscopy

ABSTRACT

$CaCl_2$ is occasionally the major or only important chloride species in natural aqueous fluid inclusions. The presence of $CaCl_2$ can be proven by a combination of Raman spectroscopy and microthermometry. Inclusions containing H_2O–$CaCl_2$ have been synthesised in quartz in order to study phase relationships and phase transitions at low temperatures. The synthetic inclusions reveal variable freezing behaviours depending on the salinity, reflecting highly metastable phase assemblages. Nevertheless, Raman spectra of antarcticite (3240 ± 2, 3387 ± 2, 3402 ± 2 and 3430 ± 1 cm^{-1}), α-tetrahydrate (3197 ± 2, 3369 ± 6, 3425 ± 3, and 3446 ± 2 cm^{-1}), γ-tetrahydrate (3435 cm^{-1}) and sinjarite (3377 ± 1, 3405 ± 3, 3424 ± 2, 3464 ± 2, 3559 ± 2 cm^{-1}) were measured at −190 °C. Final melting of ice, antarcticite and α-tetrahydrate correspond to stable phase transitions and can be used to calculate the salinity. Eutectic temperatures were not detected in this experimental study due to the absence of stable phase assemblages at low temperatures. The nucleation and melting behaviour of fluid inclusions during microthermometrical investigations can only be fully understood by Raman spectroscopic identification of the phase assemblages, either stable or metastable ones.

1. Introduction

The presence of $CaCl_2$ in aqueous solutions in individual fluid inclusions can be proved by different non-destructive qualitative methods like proton-induced X-ray emission (PIXE) (e.g. Kurosawa et al., 2003), and synchotron radiation X-ray fluorescence (SXRF) (e.g. Ménez et al., 2002). Destructive methods like semi-quantitative electron microprobe analysis (SEM/EDS), in which fluid inclusions are opened by crystal cracking and the remaining included solid phases are analysed by X-ray microanalysis (e.g. Kwak and Tan, 1981; Haynes et al., 1988), and laser-ablation inductively-coupled-plasma mass-spectroscopy (LA-ICP-MS) (e.g. Heinrich et al., 2003) have been established in the last decades. Identification of $CaCl_2$-hydrate crystals in inclusions by purely optical means, i.e. colour, habit, birefringence and refractive index (e.g. Davis et al., 1990) can be performed with large single hydrate crystals. However, this method cannot be applied to microcrystalline aggregates of hydrates and ice, which may regularly occur in frozen inclusions.

The salinity in inclusions reflects, in principle, the mole ratio of water and salts. Microthermometry is the only method, which can be used to obtain directly quantitative information on the salinity of fluid inclusions. The presence of $CaCl_2$ can be inferred from a relatively low eutectic temperature at −50 °C (e.g. Yanatieva, 1946; Crawford, 1981; Shepherd et al., 1985). Indirectly, the presence of $CaCl_2$ in fluid inclusions is suspected if relatively low eutectic temperatures, or relatively low melting temperatures of ice are obtained (e.g. Zwart and Touret, 1994; Samson and Walker, 2000). Other solutes, like $MgCl_2$ or salt mixtures, may also reveal low eutectic temperatures, which complicate the verification of the presence of $CaCl_2$ in natural inclusions. Moreover, in multi component H_2O–salt systems various complex phase assemblages may occur during freezing, which then are difficult to interpret by only using optical microscopy. Microthermometry also reveals final melting points of ice, hydrates or salts, which then allow salinity estimations using proper equations of states (see Bakker, 2003, and references therein). Phase changes observed in fluid inclusions during microthermometric experiments are only indirect indicators of the components, which are involved in e.g. melting processes. For example, the melting of ice in an aqueous solution below 0 °C indicates the presence of salt, but the type of salt, either NaCl, $CaCl_2$ or $MgCl_2$, cannot be determined from this temperature alone. Raman spectroscopy offers the possibility to identify the type of salts from hydrate phases in aqueous inclusions that appear in microthermometric experiments (Dubessy et al., 1982, 1992; Bakker, 2004).

The aim of this paper is the characterisation of Raman spectra of various $CaCl_2 \cdot 6H_2O$ hydrates (i.e. antarcticite ($CaCl_2 6H_2O$), modifications of "tetrahydrate" ($CaCl_2 \cdot 4H_2O$), and sinjarite ($CaCl_2 \cdot 2H_2O$)) in fluid inclusions synthesised in natural quartz. The different $CaCl_2$-hydrates can be distinguished by their specific Raman spectra at low temperatures. These spectra can be used as standards for comparison with spectra obtained from frozen natural fluid inclusions. Raman spectra are also obtained at various temperatures to identify phase changes in the inclusions, e.g. melting of hydrates or phase transitions

* Corresponding author. Department of Applied Geosciences, Mineralogy and Petrology, University of Leoben, Peter-Tunner Str. 5, A-8700 Leoben, Austria. Tel.: +43 3842 402 6211; fax: +43 3842 47016.
E-mail address: ronald.bakker@mu-leoben.at (R.J. Bakker).

0009-2541/$ – see front matter © 2009 Elsevier B.V. All rights reserved.
doi:10.1016/j.chemgeo.2009.04.012

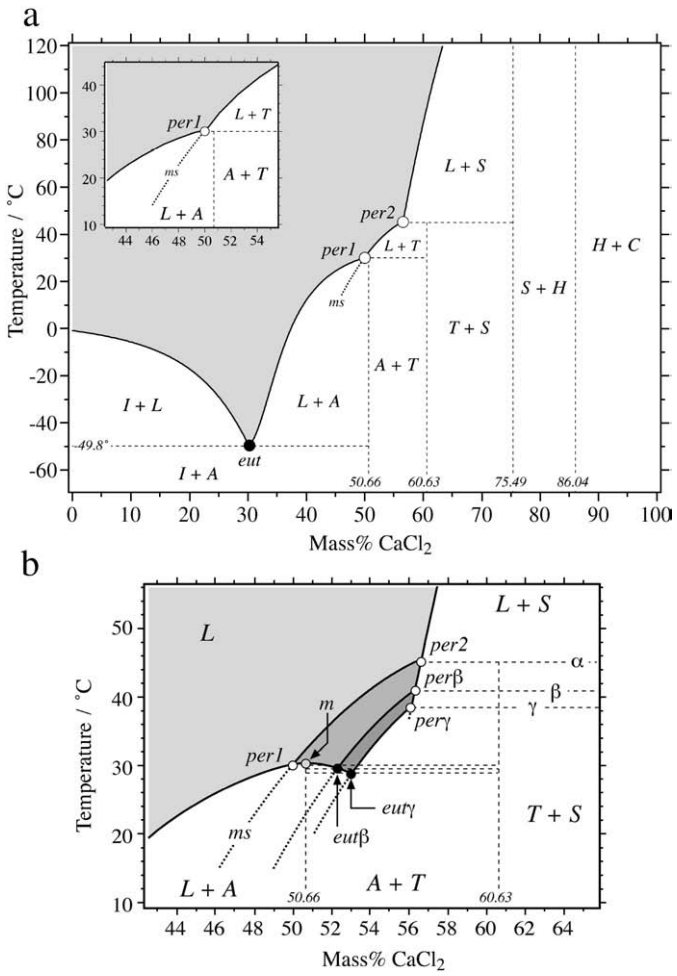

Fig. 1. a) Vapour saturated phase relations in the $CaCl_2$–H_2O system below +120 °C constructed from the solubility data presented in Linke (1957). b) Detail section of the phase relations between 42 and 66 mass% $CaCl_2$, including the α-, β- and γ-modifications of tetrahydrate. L = liquid; I = ice; A = antarcticite; T = tetrahydrate; S = sinjarite; H = $CaCl_2 \cdot H_2O$; C = $CaCl_2$; eut = eutectic; per = peritectic; ms = metastable extensions of the liquidus of α-tetrahydrate; m = maximum melt temperature at 50.66 mass% $CaCl_2$.

between hydrates, which are optically not acceptable identifiable. Additionally, the extent of metastabilities, i.e. the occurrence of metastable phase assemblages and phase changes in the H_2O–$CaCl_2$ fluid system, are determined.

2. The $CaCl_2$–H_2O system

The binary $CaCl_2$–H_2O system (e.g. Linke, 1958; Crawford, 1981) has a eutectic point at −49.8 °C (*eut* in Fig. 1a), at which the first melt forms during heating. Two peritectic points (*per1* and *per2* in Fig. 1a) with incongruently melting hydrates occur below +120 °C, where antarcticite decomposes to tetrahydrate at +30.1 °C and tetrahydrate decomposes to sinjarite at +45.1 °C. The stability fields shown in Fig. 1 are valid for a 0.1 MPa total pressure, but it can be assumed that the same phase diagram is also valid for fluid inclusions at variable pressure and at low temperatures (<+100 °C) in the presence of a vapour bubble. Polynomial best fits to the solubility data of ice (Eq. (1)), antarcticite (Eq. (2)), tetrahydrate (Eq. (3)) and sinjarite (Eq. (4)) represented in Linke (1958) are given by the following equations:

$$w = -1.9676 \cdot T - 0.064352 \cdot T^2 - 0.0011468 \cdot T^3 - 8.1 \cdot 10^{-6} \cdot T^4 \quad (1)$$

$$T = -49.8 + 1.9995 \cdot wd + 2.1473 \cdot wd^2 - 0.31895 \cdot wd^3 + 0.01986 \cdot wd^4 - 0.00058197 \cdot wd^5 + 6.521 \cdot 10^{-6} \cdot wd^6 \quad (2)$$

$$w = 45.291 - 0.01221 \cdot T + 0.0055249 \cdot T^2 \quad (3)$$

$$T = 8925.2 - 589.32 \cdot w + 13.956 \cdot w^2 - 0.14092 \cdot w^3 + 0.00051823 \cdot w^4 \quad (4)$$

where w is mass% $CaCl_2$, wd is the differential mass% ($w - 30.22$) and T is temperature in °C. Metastable extensions of the solubility curves are included in the Eqs. (2), (3) and (4). The Eqs. (1) and (3) are valid from 0 °C to −50 °C, and +15 °C to +46 °C, respectively. The Eqs. (2) and (4) are valid, from 30 to 53 mass%, and from 49 to 75 mass% $CaCl_2$. Polynomial fitting presented in Eqs. (2) and (4) cannot be performed in the reversed manner, i.e. mass% as a function of temperature, due to mathematical restrictions.

In fluid inclusions containing water and $CaCl_2$, different melting sequences of phases occur depending on the salt concentration (see also Schiffries, 1990). A fluid with a salt content less than the eutectic composition (*eut* in Fig. 1a), freezes by nucleation of ice and antarcticite below −49.8 °C. During heating, the first aqueous liquid solution forms at the eutectic temperature and where the system remains until the last antarcticite melts. Ice is the last solid phase to dissolve at temperatures dependent on the salinity. Fluid compositions between the eutectic and peritectic composition, i.e. between 30.2 and 50.0 mass% $CaCl_2$, again freeze by the nucleation of antarcticite and ice. Heating results in the complete melting of ice at the eutectic temperature, whereas antarcticite is the last phase to dissolve in the aqueous liquid solution. Within the narrow bulk compositional range between 50.0 and 50.7 mass% $CaCl_2$, i.e. at salinities lower than the composition of antarcticite, the peritectic reaction occurs at +30.1 °C, where antarcticite decomposes completely and tetrahydrate (α-modification) is formed. Tetrahydrate is the last phase to melt in the presence of an aqueous liquid solution and records the salinity of the brine. Fluids with a composition between 50.7 (*per1* in Fig. 1a) and 56.6 (*per2* in Fig. 1a) mass% $CaCl_2$, freeze by the nucleation of antarcticite and tetrahydrate. Those phases representing a stable phase assemblage up to +30.1 °C, where the first brine occurs upon heating and antarcticite completely dissolves. Therefore, the tetrahydrate is again the last solid phase to dissolve at temperatures dependent on the salinity. The different melting sequences show that small variances in salinity around 50 mass% $CaCl_2$ in inclusions can result in variable phase assemblages and different melting behaviour.

Tetrahydrate may occur in three different modifications, i.e. the α, β and γ modification (Linke, 1958). The liquidus in systems with ß- and γ-tetrahydrate is at lower temperatures than with the α-modification (Fig. 1b). Consequently, the peritectic melting conditions with antarcticite and sinjarite are significantly lowered. Incongruent melting of tetrahydrate to sinjarite occurs at +41.0 °C and +37.5 °C with the β- and γ-modification, respectively (*per*β and *per*γ in Fig. 1b). Incongruent melting of antarcticite to α-tetrahydrate (Fig. 1a) does not occur with the β- and γ-modifications. The presence of those hydrates results in the formation of a double eutectic, with a maximum temperature of the liquidus at the composition of antarcticite (*m* at +30.2 °C in Fig. 1b). These new eutectic points occur at +29.5 °C and 52.3 mass% $CaCl_2$ for the β-modification and at +29.0 °C and 53.0 mass% $CaCl_2$ for the γ-modification. Polynomial best fits to the solubility data of β-tetrahydrate (Eq. (5)) and γ-tetrahydrate (Eq. (6)) represented in Linke (1958) are given by the following equations:

$$w = 47.725 + 0.022852 \cdot T + 0.0044603 \cdot T^2 \quad (5)$$

$$w = 49.545 - 0.011960 \cdot T + 0.0049721 \cdot T^2 \quad (6)$$

where w is consistent with mass% $CaCl_2$ and T is temperature in °C. Metastable extensions of the solubility curves are included in the Eqs. (5) and (6). The Eqs. (5) and (6) are valid from +10 °C to +41 °C, and +10 °C to +38 °C, respectively. All modifications of tetrahydrate may occur in fluid inclusions during microthermometrical experiments, which may complicate the interpretation of melting and freezing behaviours.

3. Synthesis of inclusions and methods

Fluid inclusions were synthesised in thermal shock fractures in natural Brazilian quartz according to the method of Bodnar and Sterner (1987). The synthesis was performed in cold seal pressure vessels for a healing time of approximately 2 weeks (Table 1). The crack healing process takes place at about 600 °C at varying pressures between 148 and 280 MPa. The cooling down of the pressure vessels was performed along the specific isochoric path of the experiments to prevent decrepitation or stretching of the fluid inclusions. The intended salinity of the added fluid in the capsules before experimentation varies between 15 and 45 mass% $CaCl_2$ (Table 1). Experimental difficulties, e.g. the hygroscopic behaviour of $CaCl_2$-hydrates, may influence the initial weighing during the preparation of solutions for synthesis. The actual salinities in the fluid inclusions after experimentation are calculated with Eqs. (1)–(6). After synthesis the quartz core was cut in 1 mm thick sections, doubly polished and analysed with microthermometry and Raman spectroscopy.

Microthermometry measurements were carried out with a Linkam MDS 600 heating-freezing stage. Calibration was done by using synthetic fluid inclusions with the melting point of CO_2 at −56.6 °C, the melting of water at 0.0 °C and the critical homogenisation temperature of water at 374.0 °C. Different cycling runs were performed using different parameters to promote nucleation in the inclusions. Thereby different cooling/heating rates from 3°/min up to 30°/min were chosen. Subsequential heating and freezing was performed using stepwise time delays up to 1 h. Raman spectroscopy was performed with a LABRAM (ISA Jobin Yvon) instrument using a frequency-doubled 100 mW Nd-YAG laser with an excitation wavelength of λ = 532.6 nm. All measurements were taken with an LMPlanFI 100×/0.80 (Olympus) objective lens. Measurements have an accuracy of 1.62 cm^{-1} at low Δ ν (around 0 cm^{-1}) and 1.1 cm^{-1} at high Δ ν (around 3000 cm^{-1}). For internal calibration silicon (520 cm^{-1}), polyethylene (1062 cm^{-1}, 1128 cm^{-1}, 1169 cm^{-1}, 1295 cm^{-1}, 1487 cm^{-1}, 1439 cm^{-1}, 2848 cm^{-1}, 2881 cm^{-1}) and calcite (156 cm^{-1}, 283 cm^{-1}, 713 cm^{-1}, 1087 cm^{-1}, 1437 cm^{-1}) were used.

4. Freezing and melting behaviour of inclusions in the $CaCl_2$–H_2O system

Various freezing and melting behaviours are observed in synthetic fluid inclusions depending on the salinity. In addition, a variety of phase transitions and metastabilities occur within the inclusions during microthermometrical experiments.

Table 1
Experimental conditions of $CaCl_2$–H_2O synthesised fluid inclusions in quartz.

Experiment	Intended mass% $CaCl_2$	Duration [days]	P [MPa]	T [°C]
020	30	15	196.6 (±1.1)	601.0 (±0.2)
021	45	15	280.2 (±0.4)	600.1 (±1.0)
022	15	14	148.5 (±0.8)	600.3 (±0.2)
044	15	16	148.1 (±0.3)	599.8 (±0.5)
045	30	15	195.9 (±0.1)	601.2 (±0.2)

P (pressure) and T (temperature) represent the experimental conditions.

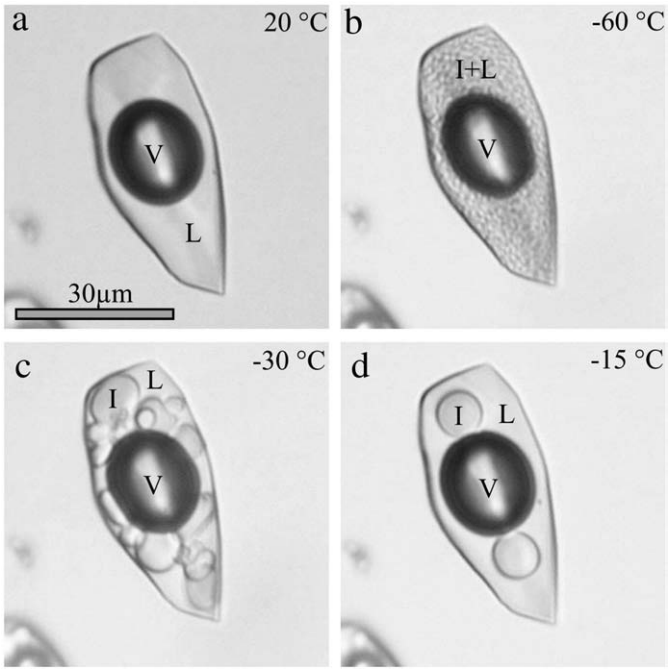

Fig. 2. Freezing and melting behaviour of a 15 mass% $CaCl_2$–H_2O fluid inclusion (Exp. 044). a) Inclusion at +20 °C, composed of brine and vapour. b) Nucleation of ice at about −60 °C, whereas brine is present in the interstitial space between the multicrystalline ice mixture. c) Recrystallised ice and brine in the presence of vapour at −30 °C. d) Single ice crystals in the presence of brine and vapour at −15 °C. V = vapour; L = liquid; I = ice.

4.1. Low saline inclusions

Inclusions with low salinities (Exp. 022 and 044), i.e. below the eutectic composition, nucleate ice in freezing experiments between −60 and −80 °C (Fig. 2a,b). Ice appears in a granular, microcrystalline texture. Antarcticite, the theoretical stable hydrate below temperatures of −49.8 °C, remains metastably absent while cooling and heating the inclusions, whereas a $CaCl_2$-rich supersaturated brine is present at all temperatures. The phase assemblage (ice, brine and vapour) is stable down to −196 °C, which is the lower limit for the heating freezing stage. No further precipitation or nucleation occurs during subsequential heating and freezing in those inclusions. Heating induces ice recrystallisation and thereby crystal enlargement (Fig. 2c,d). Last melting was obtained at about −18.4 ± 1.0 °C (Exp. 022) and at about −11.1 ± 0.2 °C (Exp. 044). Salinity calculations based on the ice melting temperatures result in 20.6 ± 0.5 mass% $CaCl_2$ and 15.3 ± 0.2 mass% $CaCl_2$, respectively.

The metastable absence of antarcticite does not allow the determination of the eutectic reaction in those fluid inclusions. Raman spectra obtained at −190 °C illustrate the presence of ice and saline aqueous solution (Fig. 3). Different cycling modes with varying cooling rates or using stepwise cooling do not affect the nucleation behaviour. Only the recrystallisation process of ice can be varied by using different cycling parameters. Slow heating results in the growth of large single ice crystals in the solution, whereas rapid heating inhibits the recrystallisation of small ice crystals and numerous small crystals remain present until the final stages of melting.

4.2. Eutectic composition

Inclusions with salinities near to the eutectic composition (Exp. 020 and 045) seldomly nucleate ice during cooling experiments, whereas antarcticite is always metastably absent. In only a few inclusions from

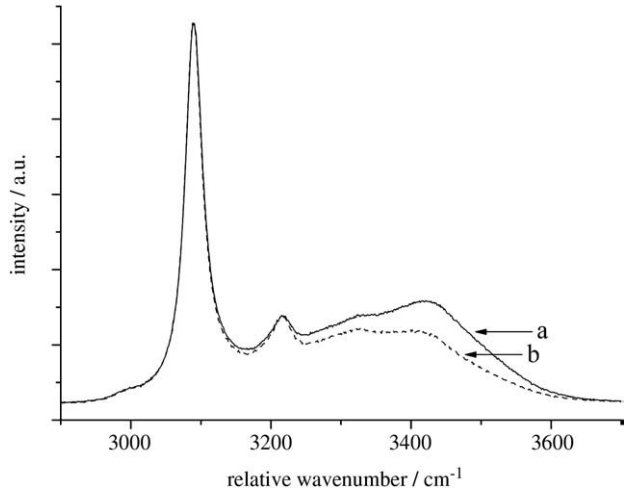

Fig. 3. Raman spectrum of (*a*) ice/brine in comparison with a Raman spectrum of (*b*) ice, obtained from a 15 mass% $CaCl_2$–H_2O fluid inclusion at −190 °C (Exp. 044). The presence of brine is verified with an increase in intensity at wavenumbers between 3250 and 3600 cm^{-1}.

experiment 045, ice nucleated, which melted at -46.5 ± 0.3, corresponding to salinity of 29.8 ± 0.1 mass% $CaCl_2$. More typically, an undercooled saline liquid remains present with the vapour phase down to −190 °C in those fluid inclusions. A relative increase in the volume fraction (about 6%) of the vapour phase is observed (c.f. Bakker and Diamond, 2006). The application of different cycling parameters does not influence the absence of nucleation in the inclusions. Subsequent cooling and heating of inclusions does not induce crystallisation. Raman spectroscopic analyses reveal the metastable existence of brine at temperatures below the eutectic point. The spectral evolution of the supercooled brine was obtained at different temperatures (Fig. 4) and illustrates a noteworthy change in shape at lower temperatures.

4.3. High saline inclusions

Minor variations in salinity and unpredictable metastabilities result in different types of hydrate nucleation in highly saline synthetic inclusions. For example, four types of hydrate nucleation are observed in fluid inclusions with a salinity at about 50 mass% $CaCl_2$ from experiment 021.

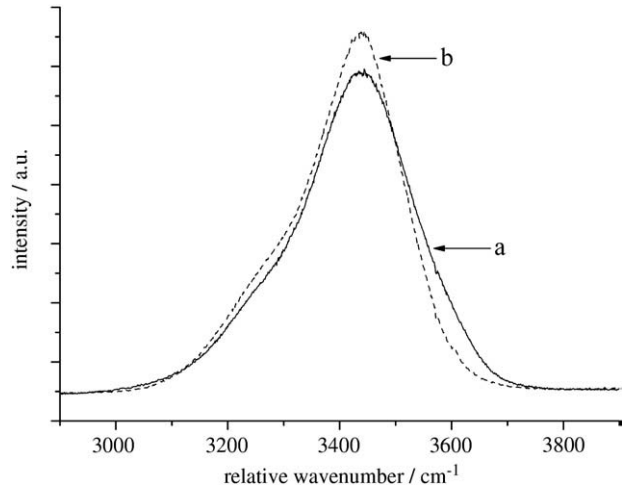

Fig. 4. Raman spectrum of a brine with eutectic composition (*a*) at room temperature and (*b*) at −190 °C (Exp. 020).

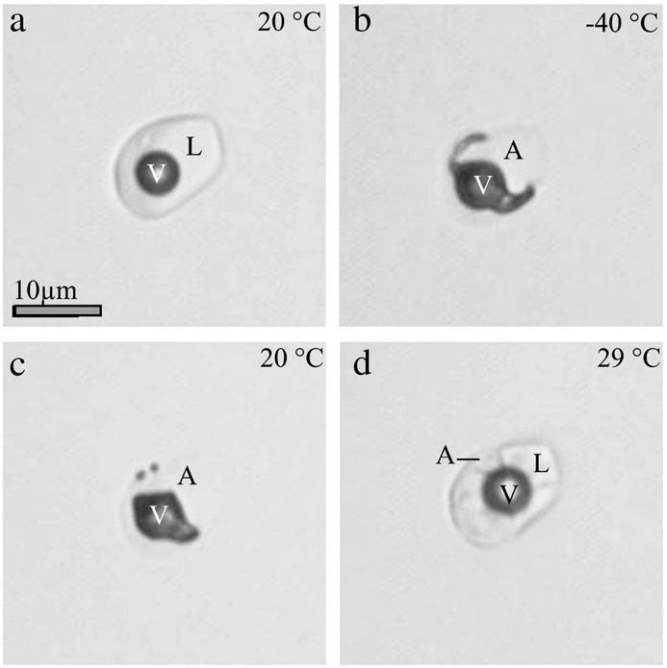

Fig. 5. Freezing and melting behaviour of a 50 mass% $CaCl_2$–H_2O fluid inclusion (Exp. 021). a) Inclusion at +20 °C, composed of brine and vapour. b) Nucleation of antarcticite at about −40 °C. c) Recrystallised antarcticite and brine in the presence of vapour at +20 °C. d) Single antarcticite crystals in the presence of brine and vapour at +29 °C. V = vapour; L = liquid; A = antarcticite.

4.3.1. Antarcticite ($CaCl_2 \cdot 6H_2O$)

Nucleation of antarcticite occurs in a temperature range between −40 °C and −65 °C during cooling experiments (Fig. 5a,b). The vapour bubble deforms intensely due to the nucleation. The hydrate is glassy at this temperature and has a similar refractive index to quartz (Fig. 5b). The bulk salinity of the inclusion is close to the composition of antarcticite, therefore, the amount of ice (or rather liquid) is expected to be very small. The phase assemblage (i.e. antarcticite, vapour and potentially a small amount of ice or liquid) remains stable down to −190 °C. Neither ice nor liquid are identifiable with Raman spectroscopy. Raman spectroscopy verifies the presence of antarcticite with four main peak positions at 3240 ± 2, 3387 ± 2, 3402 ± 2 and 3430 ± 1 cm^{-1} at −190 °C (Fig. 6). At higher temperatures, the peaks

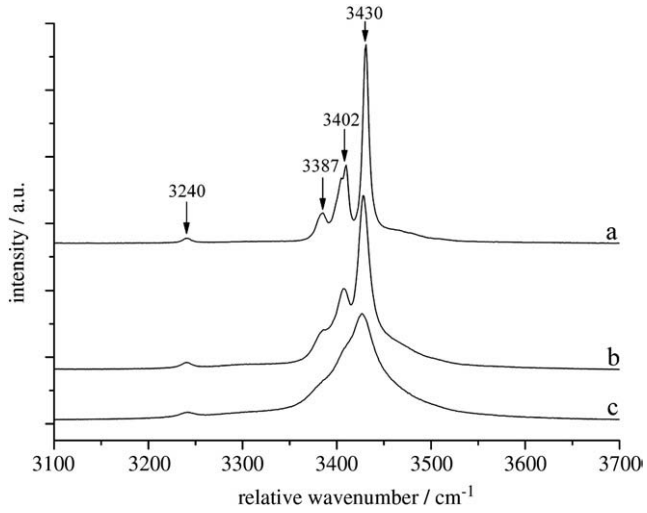

Fig. 6. Raman spectra of antarcticite at (a) −190 °C, (b) −100 °C and (c) +20 °C (Exp. 021).

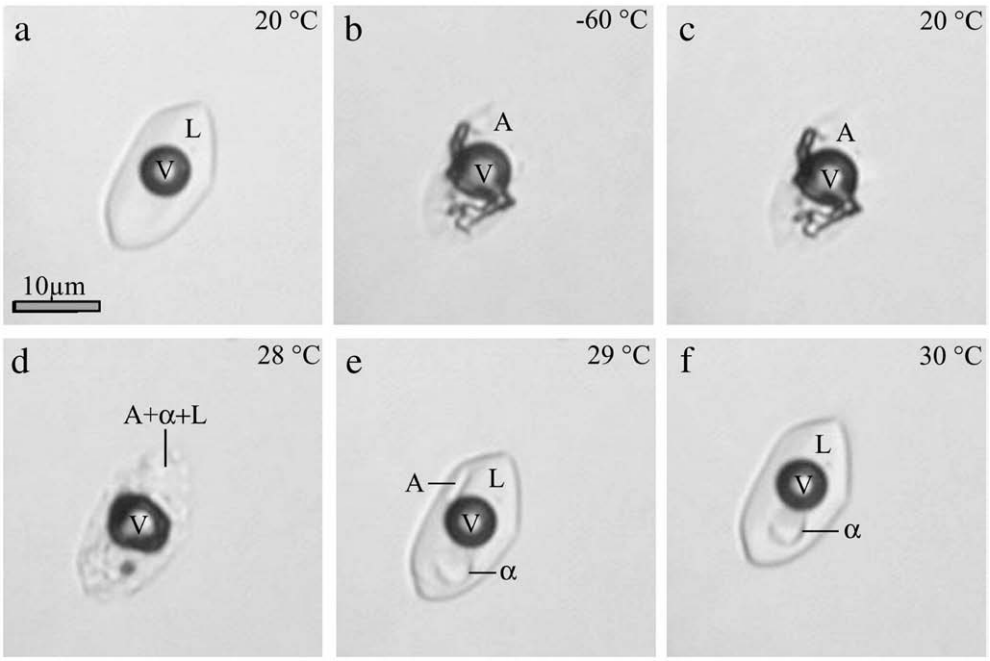

Fig. 7. Freezing and melting behaviour of a 50 mass% $CaCl_2$–H_2O fluid inclusion (Exp. 021). a) Inclusion at +20 °C, composed of brine and vapour. b) Nucleation of antarcticite at about −60 °C. c) Recrystallised antarcticite and brine in the presence of vapour at +20 °C. d) Antarcticite, α-tetrahydrate, brine and vapour at +28 °C (start of the peritectic reaction). e) Single crystals of antarcticite and α-tetrahydrate in the presence of brine and vapour at +29 °C. f) α-tetrahydrate, brine and vapour at +30 °C, whereas antarcticite is already dissolved. V = vapour; L = liquid; A = antarcticite; α = α-tetrahydrate.

are less well defined and spectroscopic details are lost. During heating, reactions (including phase changes) are not observable in the inclusions. Small movements of the "deformed" vapour phase may occur due to recrystallisation, whereas melting processes are not observed (Fig. 5b,c). First optically visible melting is observed at about +28 °C. Thereby, single antarcticite crystals are formed (Fig. 5d), which dissolve in a small temperature range. The last melting was observed at about +29.4 ± 0.3 °C. This melting temperature implies a calculated salinity of 49.0 ± 0.5 mass% $CaCl_2$, close to the peritectic point at 50.7 mass% $CaCl_2$.

4.3.2. Antarcticite ($CaCl_2 \cdot 6H_2O$) and α-tetrahydrate (α-$CaCl_2 \cdot 4H_2O$)

Similar to the previously described freezing behaviour, antarcticite nucleates in synthetic fluid inclusions again in the temperature range between −40 °C and −65 °C (Fig. 7a,b). The vapour bubble deforms at the nucleation temperature and reactions are not observable at temperatures between −190 °C and +28 °C (Fig. 7c). During further heating, the peritectic reaction takes place at about +29 °C and thereby α-tetrahydrate and large amounts of liquid are formed (Fig. 7d,e). At +30 °C, α-tetrahydrate, brine and vapour represent a stable phase assemblage, whereas antarcticite is completely consumed by the

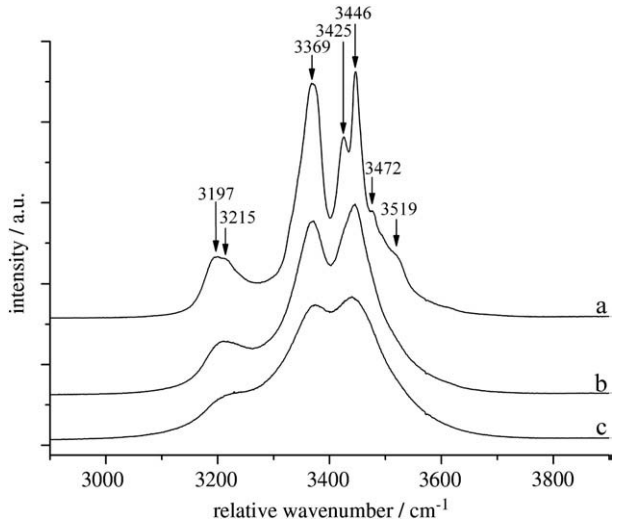

Fig. 8. Raman spectra of α-tetrahydrate at (a) −190 °C, (b) −100 °C and (c) 0 °C (Exp. 021).

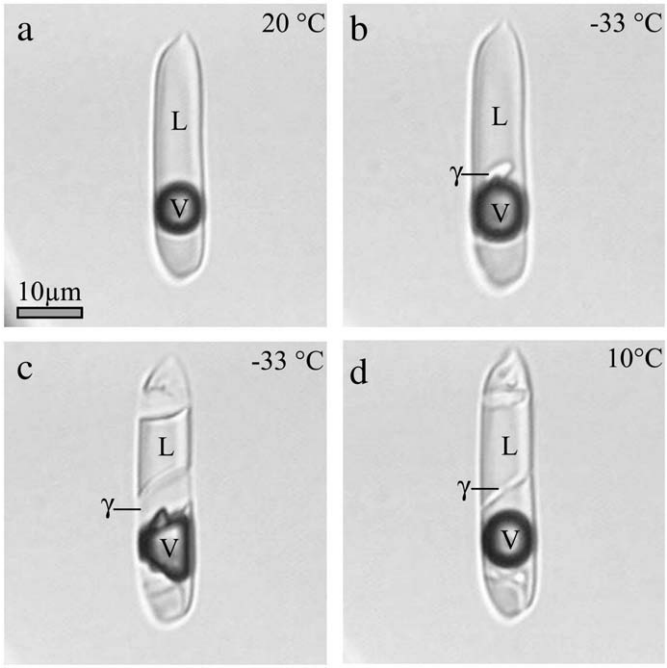

Fig. 9. Freezing and melting behaviour of a 50 mass% $CaCl_2$–H_2O fluid inclusion (Exp. 021). a) Inclusion at +20 °C, composed of brine and vapour. b) Nucleation of γ-tetrahydrate at about −33 °C. c) Growing of γ-tetrahydrate crystals by holding a constant temperature of −33 °C. d) γ-tetrahydrate in the presence brine and vapour at +10 °C. V = vapour; L = liquid; γ = γ-tetrahydrate.

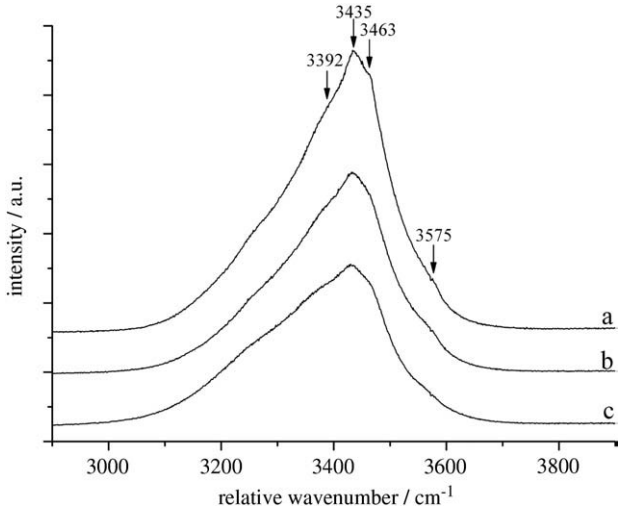

Fig. 10. Raman spectra of γ-tetrahydrate at (a) −190 °C, (b) −100 °C and (c) −27 °C (Exp. 021).

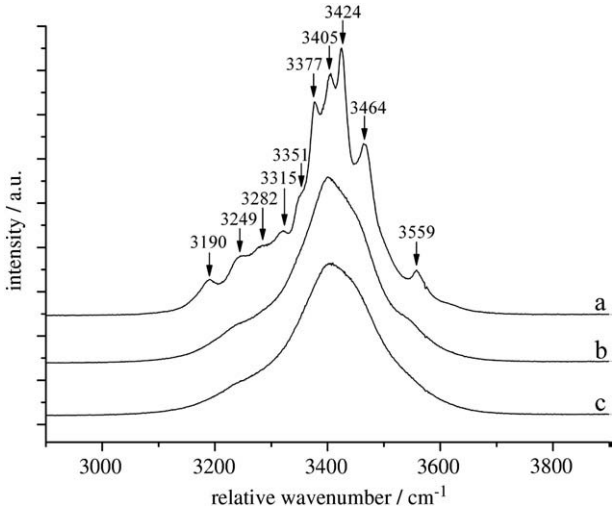

Fig. 12. Raman spectra of sinjarite at (a) −190 °C, (b) −100 °C and (c) −50 °C (Exp. 021).

reaction (Fig. 7e,f). Cooling of this phase assemblage to temperatures below the peritectic point results in the growth of α-tetrahydrate crystals in the metastable absence of antarcticite. Subsequently, α-tetrahydrate can be measured with Raman spectroscopy in this metastable phase assemblage at −190 °C (Fig. 8). Raman spectra of the α-modification reveal main peak positions at 3197 ± 2, 3369 ± 6, 3425 ± 3, and 3446 ± 2 cm^{-1}. Shoulders, i.e. probably hidden peaks, can be defined at approximately 3215 ± 64, 3472 ± 5, and 3519 ± 2 cm^{-1}. The last melting in those inclusions is observed at 32.5 ± 0.4 °C with the dissolution of α-tetrahydrate, which corresponds to a calculated salinity of 50.7 ± 0.1 mass% $CaCl_2$.

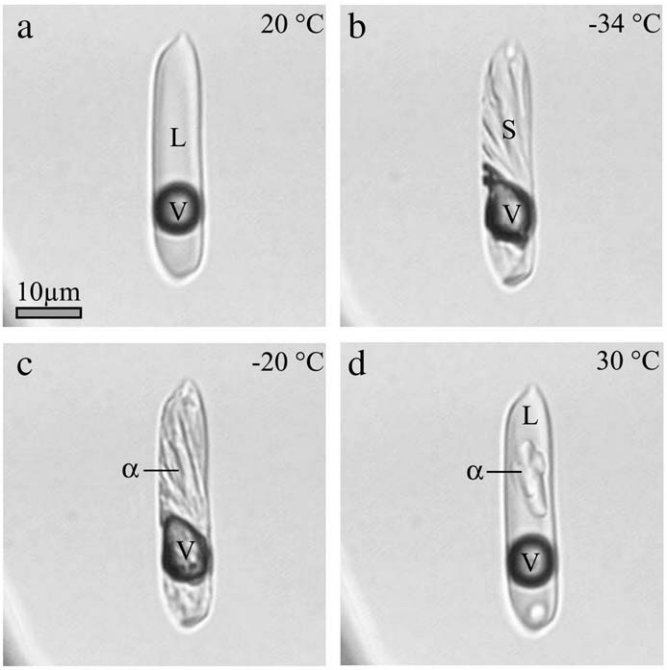

Fig. 11. Different freezing and melting behaviour in the same inclusion as illustrated in Fig. 9 (Exp. 021). a) Inclusion at +20 °C, composed of brine and vapour. b) Nucleation of sinjarite at about −34 °C. c) Inclusion at −20 °C composed of α-tetrahydrate (after the phase transition of sinjarite into α-tetrahydrate). d) α-tetrahydrate in the presence of brine and vapour at +30 °C. V = vapour; L = liquid; S = sinjarite; α = α-tetrahydrate.

4.3.3. γ-Tetrahydrate (γ-$CaCl_2 \cdot 4H_2O$)

At temperatures of about −30 °C, hydrate crystals may nucleate and grow slowly at a constant low temperature (Fig. 9a,b,c). The final melting temperature of this hydrate is observed at +11.5 ± 0.2 °C (Fig. 9d). The phase assemblage including the hydrate, brine and vapour remains present down to −190 °C. At this temperature, Raman spectra of this hydrate phase does not show well defined peaks, but resembles a "deformed" aqueous liquid solution, with a main peak position at about 3435 cm^{-1} (Fig. 10). Hidden peaks, respectively shoulders can be defined at about 3392, 3463 and 3575 cm^{-1}, which vary over a range of relative wavenumber. The evolution of the Raman spectrum of this hydrate at various temperatures is illustrated in Fig. 10. It is assumed that the Raman spectrum from Fig. 10 corresponds to a poorly crystallised γ-modification of tetrahydrate. The final melting temperature of this hydrate phase corresponds to the metastable extension of the liquidus with γ-tetrahydrate. The corresponding calculated salinity (Eq. (6)) is 50.1 ± 0.0 mass% $CaCl_2$.

4.3.4. Sinjarite ($CaCl_2 \cdot 2H_2O$) and α-Tetrahydrate (α-$CaCl_2 \cdot 4H_2O$)

Within the same fluid inclusion illustrated in Fig. 9, a different freezing behaviour can be observed by the nucleation of another metastable hydrate phase at about −35 °C (Fig. 11a,b). This phase appears to replace completely the brine in the fluid inclusions. A residual liquid phase could not be optically or spectroscopically

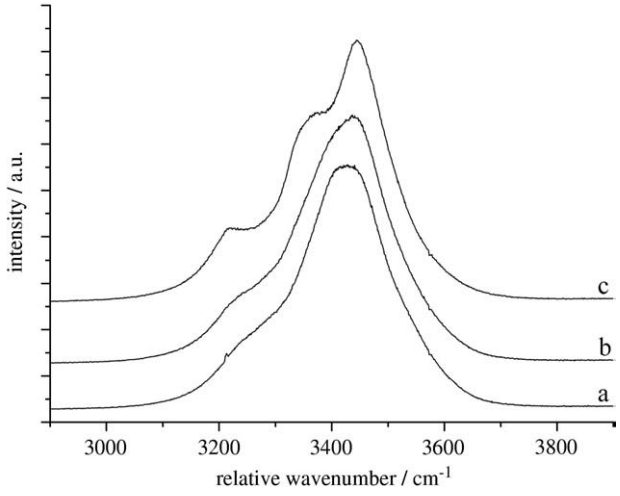

Fig. 13. Raman spectra, displaying the phase transition sinjarite to α-tetrahydrate, taken at (a) −30 °C, (b) −28 °C and (c) −26 °C (Exp. 021). See text for further details.

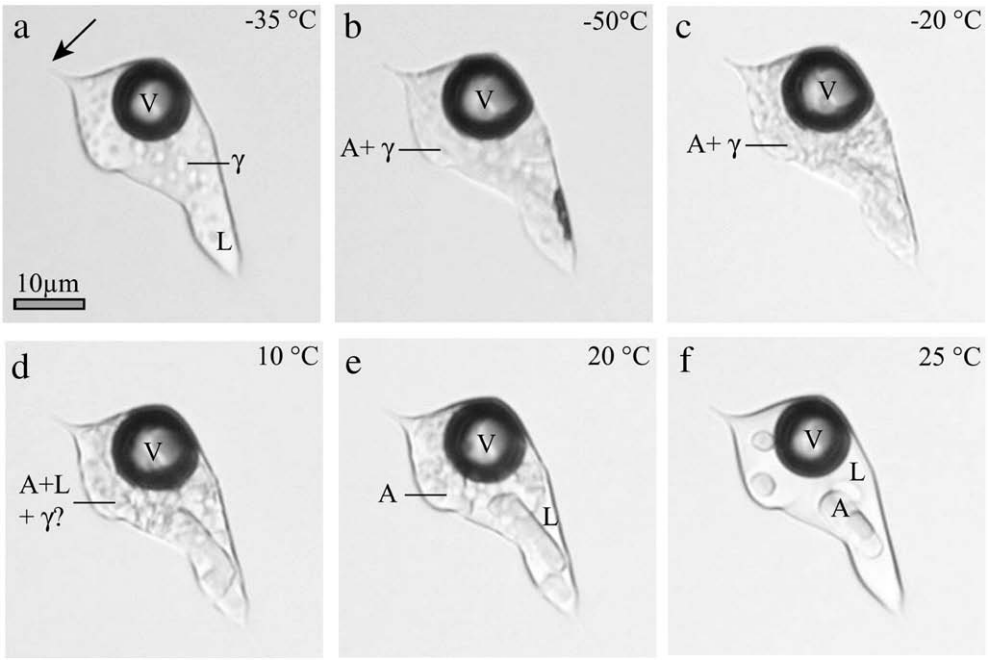

Fig. 14. Freezing and melting behaviour of a fluid inclusion, whose formation resulted from incomplete crack healing (Exp. 045). The arrow marks a fine channel, through which the inclusion is still connected to unsealed cracks. a) Nucleation of γ-tetrahydrate at about −35 °C. b) Nucleation of antarcticite at about −50 °C, whereas γ-tetrahydrate is still present. c) Recrystallised γ-tetrahydrate and antarcticite in the presence of vapour at −20 °C. d) Antarcticite, brine and probably γ-tetrahydrate at +10 °C. e) Antarcticite and brine at +20 °C, whereas γ-tetrahydrate has already melted. f) Single antarcticite crystals in equilibrium with brine and vapour at + 25 °C. V = vapour; L = liquid; A = antarcticite; γ = γ-tetrahydrate.

verified, but a small amount of liquid cannot be excluded to be present with the hydrate and may occur as a thin film between hydrate crystals. Further cooling of the inclusion does not promote any reaction or recrystallisation and this phase assemblage is present down to −190 °C. Raman spectra at this temperature display a complex contour with main peak positions at 3377 ± 1, 3405 ± 3, 3424 ± 2, 3464 ± 2, 3559 ± 2 cm^{-1} (Fig. 12). Shoulders, (i.e. hidden peaks) can be defined at 3190 ± 2, 3249 ± 9, 3282 ± 4, 3315 ± 5 and 3351 ± 4 cm^{-1}. The Raman spectral peaks and shoulders are smoothed to a single broad spectrum at higher temperatures, resembling again a "deformed" water spectrum (Fig. 12b,c). During heating, a phase transition into α-tetrahydrate takes place in a temperature range between −29 and −25 °C. The phase transition is accompanied with a slight coarsening in the crystal texture, without the formation of an aqueous liquid (Fig. 11b,c), and is optically difficult to observe. The transition is evident by a change in the Raman spectra of the hydrate phase (Fig. 13). At −30 °C the Raman spectra is characterised by a broad undefined peak, similar to Fig. 12c. Heating to −26 °C results in a spectrum with slightly more pronounced peaks and shoulders. This behaviour is not expected for simple hydrates, because increasing temperatures are usually smoothing the spectra (see Figs. 6 and 12). This phase transition is metastably irreversible, and the Raman spectra, subsequently, obtained at −190 °C are equivalent to the α-tetrahydrate, as illustrated in Fig. 8. The last melting of α-tetrahydrate is observed at about +32.5 ± 0.4 °C. The hydrate phase illustrated in Fig. 12 is assumed to be a sinjarite, because the temperature of phase transition corresponds to the metastable extension of the liquidus of sinjarite at about 50 mass% $CaCl_2$. As both, the spectra of α-tetrahydrate and sinjarite are very complex and the background signal is relatively high in the range of 3200 to 3600 cm^{-1}, it is likely that a liquid phase is present throughout the observed temperature range.

4.3.5. Peculiarities

Incomplete crack healing in experiment 045 resulted in the formation of fluid inclusions that are not completely isolated and still connected with fine channels to the quartz surface (arrows in Figs. 14 and 16). Capillary forces inhibit the complete loss of the fluid from these inclusions. Probably, water has been predominantly lost through those channels, because the inclusions reveal a higher salinity than the intended 30 mass% $CaCl_2$. Consequently, those inclusions reveal a similar freezing behaviour to inclusions from experiment 021 (50 mass% $CaCl_2$). The nucleation of small hydrate crystals (γ-tetrahydrate) at about −35 °C (Fig. 14a) corresponds to the observation from experiment 021 (see Section 4.3.3.). A second nucleation (antarcticite) takes place by heating and freezing of the fluid inclusions at various temperatures (Fig. 14b), in contrast to the observations in the inclusions from experiment 021. This phase assemblage is present down to −190 °C. The Raman spectra gained at −190 °C, resemble a combination of the γ-tetrahydrate and antarcticite (Fig. 15). Heating results in recrystallisation (Fig. 14c,d,e) and

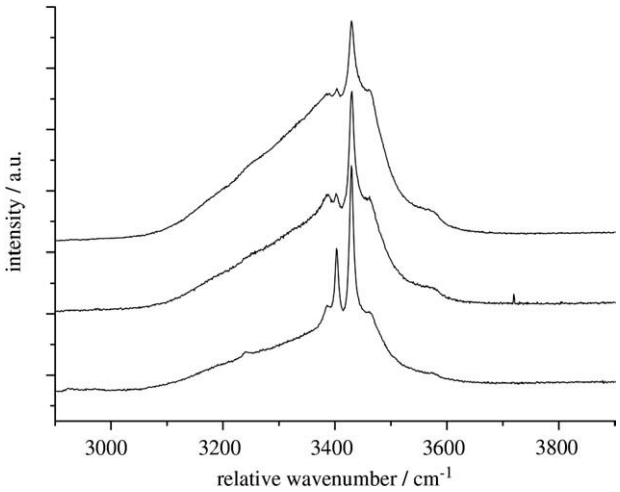

Fig. 15. Raman spectra, which resemble the presence of γ-tetrahydrate and antarcticite at −190 °C (Exp. 045).

therefore the occurrence of first melt is difficult to obtain. Also, the final melting temperature of the γ-tetrahydrate in the presence of antarcticite is optically not evident. Above −190 °C, the Raman spectrum of the γ-tetrahydrate can easily be confused with the spectrum of a brine at low temperatures, due to its poorly crystalline properties. Additionally, antarcticite with its strong Raman bands, camouflage the Raman signals of the γ-tetrahydrate. During several cycling experiments it was possible to observe the melting behaviour of γ-tetrahydrate without any nucleation of antarcticite. The last melting of γ-modification was obtained in a temperature range between +5 and +11 °C, similar to those temperatures observed in experiment 021. The final melting of antarcticite occurs at +25.4± 0.8 °C, corresponding to a calculated salinity of 45.7±0.5 mass% $CaCl_2$.

Secondly, in other incompletely healed fluid inclusions from experiment 045, nucleation of a clear glassy phase may occur at about −50 °C (Fig. 16a,b), similar to the behaviour illustrated in Fig. 5. The phase replaces completely the brine and is only evident by a slight deformation of the vapour bubble (Fig. 16b). The glassy phase recrystallises during subsequent heating into a microcrystalline mixture (orange-skin texture) at −20 °C (Fig. 16c), and finally to larger single crystals of antarcticite (Fig. 16d). During cooling, these crystal grow constantly down to −190 °C in the presence of an undersaturated brine (Fig. 16e,f). Last melting of antarcticite was also observed at 25.5±0.4 °C, corresponding to 45.7±0.3 mass% $CaCl_2$.

5. Discussion

Schiffries (1990) has identified antarcticite crystals in liquid-absent natural fluid inclusions from mafic pegmatites (Bushveld) by Raman spectroscopy. Furthermore, halite was identified by optical methods at room temperatures. Theoretically, these inclusions should also contain tetrahydrate, however, metastabilities among the α-, β- and γ-modifications did not allow an unequivocal interpretation of the Raman spectra obtained in the range of 1600 to 1700 cm^{-1}, whereas only antarcticite was identified in the range of 2800 to 3800 cm^{-1}. Analyses of natural $CaCl_2$-bearing fluid inclusions in quartz, halite, fluorite and calcite (Davis et al., 1990; Schiffries, 1990; Zwart and Touret, 1994; Samson and Walker, 2000) were interpreted in a ternary H_2O–NaCl–$CaCl_2$ fluid system. In these studies, the presence of $CaCl_2$ could not be verified by direct means, i.e. Raman spectroscopy, but was only inferred from relatively low melting temperatures in the inclusions.

Eutectic temperatures are normally used to define the salt system in natural fluid inclusions. The assumption for this application is the presence of stable phase assemblages and reliable data of phase relationships. Hydrate nucleation, especially, in low salinity inclusions are often inhibited as shown in this study. Thereby no eutectic melting occurs. Recrystallisation processes of ice or hydrates may be misinterpreted as eutectic reactions, specially, in low or high saline inclusions, where the volume fraction of ice or hydrates is relatively high. Small amounts of brine may be still present with ice and thereby those systems are not representing a stable phase assemblage. If eutectic reactions occur, it is still difficult to obtain the temperature of the first liquid produced. The first optically visible liquid may not reflect the eutectic (first) melting. Recrystallisation processes or simply poor microscopical resolution may lead to misinterpretation of eutectic processes. The eutectic points of multiple salt systems occur in a relatively small temperature range (e.g. binary $CaCl_2$–H_2O −49.8 and ternary $CaCl_2$–KCl–H_2O −50.5 °C; Borisenko, 1977) and therefore accurate melting temperatures are necessary to avoid wrong interpretations of the salt composition. Moreover, multiple salt systems complicate the investigation of reaction points (eutectic and peritectic reactions), due to the occurrence of various salt-hydrates and still unavailable solubility data. Borisenko (1977) suggests the determination of eutectic temperatures by determining thawing temperatures. This presupposes subsequent heating and freezing of fluid inclusions and the presumption of stable phase nucleation. As shown in this study, freezing of inclusions in the binary $CaCl_2$–H_2O system generally leads to metastable phase relationships. However, final melting temperatures of ice and $CaCl_2$-hydrates are still reliable indicators of the salinity of those inclusions and can be used for salinity calculation.

Samson and Walker (2000) prepared standard solutions of H_2O–NaCl–$CaCl_2$ fluids to obtain reference Raman spectra of hydrates at low

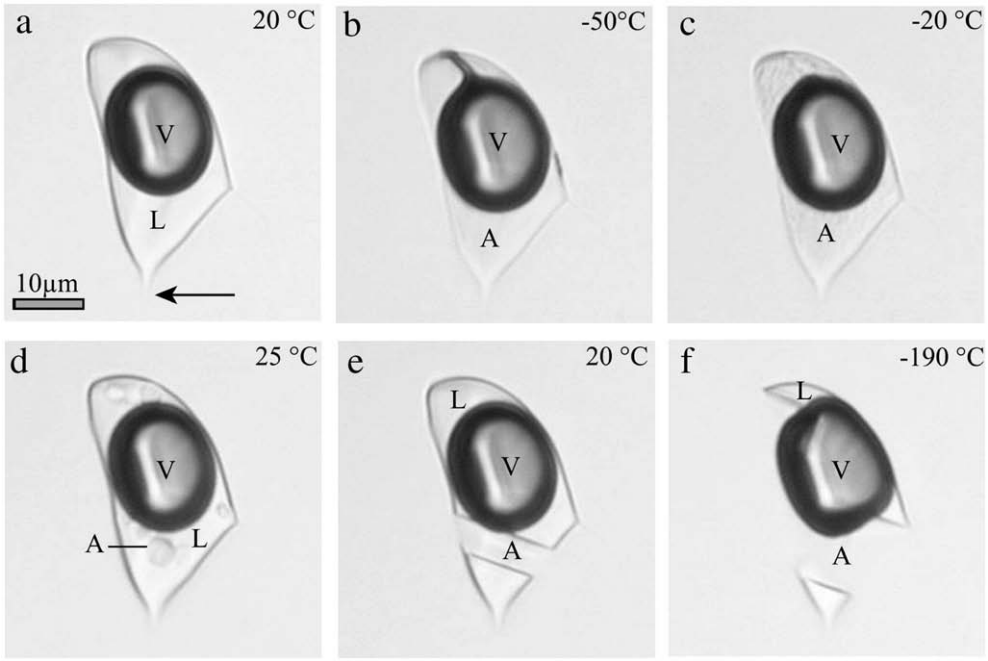

Fig. 16. Freezing and melting behaviour of a fluid inclusion, whose formation resulted from incomplete crack healing (Exp. 045). The arrow marks a fine channel, through which the inclusion is still connected to unsealed cracks. a) Inclusion at +20 °C, composed of brine and vapour. b) Nucleation of a glassy phase at about −50 °C. c) Recrystallised antarcticite in the presence of vapour at −20 °C. d) Antarcticite and brine in the presence of vapour at +25 °C. e) Single antarcticite crystal and brine in the presence of vapour at +25 °C f) Single antarcticite crystals in equilibrium with brine and vapour at −190 °C. V = vapour; L = liquid; A = antarcticite.

temperatures showing the dependence on the NaCl/$CaCl_2$ mass ratio. In contrast to our synthetic fluid inclusions samples, antarcticite crystallised in those experimental solutions below the eutectic composition (20 mass% $CaCl_2$). Our experimental work has illustrated that antarcticite only nucleates in highly saline inclusions. The relative orientation of hydrate crystal to the incident Raman laser beam has an important effect on the intensities of the individual Raman peaks (see Bakker, 2004), and these variable intensities may have an important effect on the morphology (the visibility of peaks) of Raman spectra of mixtures of hydrohalite and antarcticite.

Our experiments have revealed that metastable phase assemblages and transitions occur more often than stable conditions in inclusions containing a H_2O–$CaCl_2$ fluid mixture. Synthetic fluid inclusions containing H_2O–NaCl–$CaCl_2$ (Vanko et al., 1988) have also revealed metastable phase behaviour at low temperature, similar to our results with binary H_2O–$CaCl_2$ fluids. Those previous works illustrate, that $CaCl_2$ containing inclusions are strongly influenced by metastable processes, i.e. expected phase nucleations are absent and rather metastable phase assemblages are present.

At relative low salinities, i.e. lower than the eutectic composition, ice and brine reflect a metastable phase assemblage below the eutectic temperature. Consequently, the brine is highly oversaturated in $CaCl_2$ at −190 °C. Different behaviour is observed in inclusions with the eutectic composition: Nucleation of both ice and antarcticite are inhibited even down to −190 °C. Therefore a liquid phase may be present at extreme low temperatures (c.f. H_2O–$MgCl_2$ brines in Bakker, 2004) in inclusions and in small pores. The lack of the stable presence of antarcticite at low temperatures in inclusions from experiments 021, leads to a variety of metastable behaviour. Repression of antarcticite nucleation in highly saline inclusions may result in the formation of other $CaCl_2$ hydrates such as γ-tetrahydrate and sinjarite (see Sections 4.3.3 and 4.3.4.). These phases have distinctively different Raman spectra compared to antarcticite and α-tetrahydrate (Figs. 10 and 12). The identification of the hydrates was obtained from the metastable extensions of the liquidi, given by Eqs. (4) and (6) and the observed temperatures of phase transitions in the inclusions (Fig. 17). The γ-tetrahydrate and an undersaturated brine may represent a metastable phase assemblage down to −190 °C. It melts at about +11 °C in a bulk fluid composition of about 50 mass% $CaCl_2$ (*X* in Fig. 17a). Antarcticite was not produced after melting of the γ-tetrahydrate, therefore the phase assemblage altered into another metastability, i.e. only an undercooled brine. Secondly, the presence of sinjarite was also inferred from the metastable extensions of the liquidus (*Y* in Fig. 17b). Theoretically, the stability of sinjarite is limited within the 60.63 to 86.06 mass% $CaCl_2$ bulk composition range. However, at 50 mass% $CaCl_2$ the metastable extended liquidus of sinjarite occurs at the observed phase transition temperature between −29 and −25 °C. Most likely sinjarite is present with brine at −190 °C, but also a co-existence with γ-tetrahydrate cannot be excluded. Brine and the poorly crystallised γ-tetrahydrate are not easily to distinguished by the use of Raman spectroscopy, even in the presence of a hydrate (sinjarite), which shows intense and complex vibrational modes. After melting of sinjarite, α-tetrahydrate is produced instead of a brine along the metastable liquidus, whereas antarcticite remains metastably absent. Theoretically, antarcticite/brine or α-tetrahydrate/antarcticite represents a stable phase assemblage in this temperature range. It can be concluded that the system moves from a "strongly" metastable arrangement (sinjarite) into a "lesser" metastable one (α-tetrahydrate). The presence of sinjarite is extended to a temperature range between −190 to about −30 °C.

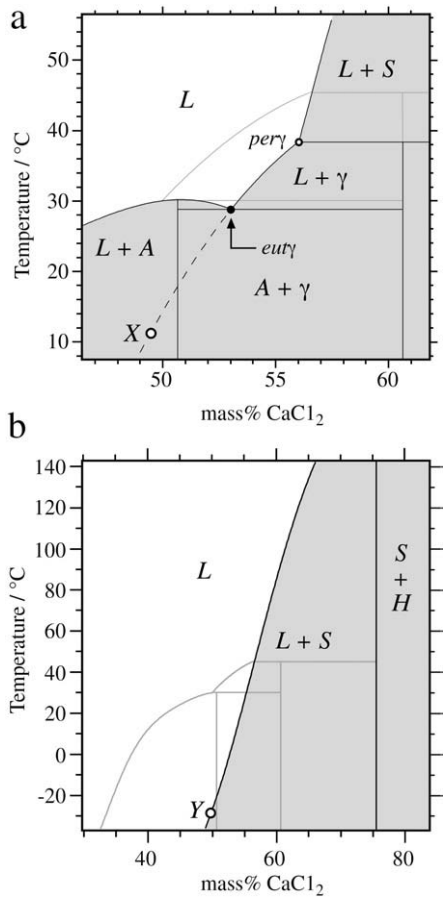

Fig. 17. Metastable phase relationship in the system H_2O–$CaCl_2$. a) Detail section with γ-tetrahydrate. The dotted line illustrates the metastable extensions of the liquidus, which intersect with the observed melting temperature of γ-tetrahydrate (*X*). b) Detail section with sinjarite. The metastable extensions of the liquidus intersect the temperature range, where the phase transition sinjarite into α-tetrahydrate was observed (*Y*). Gray lines correspond to the stable phase assemblage illustrated in Fig. 1a. L = liquid; A = antarcticite; γ = γ-tetrahydrate; S = sinjarite; H = $CaCl_2H_2O$; eut = eutectic; per = peritectic.

In H_2O–$CaCl_2$ bearing fluid inclusions, stable phase assemblages occur only close to the final melting temperatures either of ice, antarcticite, or α-tetrahydrate. Therefore, those temperatures can well be used to calculate salinity if the melting phase can be identified. The salinity of the brine in experiment 021 is close to the composition of antarcticite, and therefore small variations in experimental conditions that affect fluid composition may lead to different behaviours. Only small amounts of ice or tetrahydrate are produced at low temperatures and eutectic melting cannot be observed. Therefore, it is not possible to verify the existence of stable and metastable phase assemblages at low temperatures. Typically, these inclusions undergo the peritectic reaction and α-tetrahydrate is formed (see also Schiffries, 1990). From the data of Linke (1958) the peritectic reaction is anticipated at +30.1 °C. However, it occurs in a temperature interval between +29 and +31 °C in the synthetic fluid inclusions and thus may occur slightly prematurely or even slightly delayed. In a few cases antarcticite melts just below the peritectic temperature, which may indicate slight variances in salinity in the synthesised inclusions or rather that the peritectic reaction is inhibited.

6. Conclusions

Four types of metastable nucleation and melting behaviour are observed in synthetic H_2O–$CaCl_2$ fluid inclusions in quartz depending on the salinity: a) ice nucleation (< eutectic composition); b) lack of nucleation (eutectic composition); c) antarcticite nucleation (<50 mass% $CaCl_2$); d) complex nucleation (~50 mass% $CaCl_2$), including the crystallisation of γ-tetrahydrate and sinjarite in highly metastable phase assemblages.

All experiments have illustrated, that the fluid inclusions behave highly unpredictably at low temperatures, due to the regular formation

of metastable phase assemblages. Consequently, eutectic temperatures of fluid mixtures cannot be obtained by microthermometric investigations. Final melting always occurred in stable phase assemblages, and the temperatures can be used to calculate salinity if the melting phase can be identified as ice, antarcticite and α-tetrahydrate.

The $CaCl_2$ hydrates can be distinguished by Raman spectroscopical means due to the occurrence of characteristic vibrational modes in the range between 3000 and 3800 cm^{-1} (stretching region of water) at −190 °C. The spectrum of antarcticite reveals four main peak positions at 3240 ± 2, 3387 ± 2, 3402 ± 2 and 3430 ± 1 cm^{-1}. Characteristic main peak positions for α-tetrahydrate are defined at 3197 ± 2, 3369 ± 6, 3425 ± 3, and 3446 ± 2 cm^{-1}. The γ-tetrahydrate spectrum resembles a "deformed" aqueous liquid solution spectrum with a main peak position at about 3435 cm^{-1}. A complex spectra morphology is gained from sinjarite with characteristic main peak positions at 3377 ± 1, 3405 ± 3, 3424 ± 2, 3464 ± 2, 3559 ± 2 cm^{-1}.

Raman spectroscopy offers the only possibility to identify phases and phase assemblages in fluid inclusions during microthermometrical experiments. The phase transitions, e.g. final melting, can only be fully understood by Raman spectral identification of the phase. Because eutectic points remain hidden due to metastability, the type of dissolved salt in water can only be identified by analyses of salt hydrate spectra in frozen inclusion.

Acknowledgements

The research work is funded by the Austrian Science Fund (FWF, P18209-B06). P. Brown and an anonymous reviewer are kindly acknowledged for their help to improve this paper.

References

Bakker, R.J., 2003. FLUIDS1. Computer programs for analysis of fluid inclusion data and modelling fluid properties. Chemical Geology 194, 3–23.

Bakker, R.J., 2004. Raman spectra of fluid inclusions and crystal mixtures in the system H_2O, H_2O–NaCl and H_2O–$MgCl_2$ at low temperatures: applications to fluid inclusion research. The Canadian Mineralogist 42, 1283–1314.

Bakker, R.J., Diamond, L.W., 2006. Estimation of volume fractions of liquid and vapour phases in fluid inclusions, and definition of inclusions shape. American Mineralogist 91, 635–657.

Bodnar, R.J., Sterner, S.M., 1987. Synthetic fluid inclusions. In: Ulmer, G.C., Barnes, H.L. (Eds.), Hydrothermal Experimental Techniques. John Wiley & sons, New York, pp. 423–457.

Borisenko, A.S., 1977. Study of the salt composition of solutions of gas–liquid inclusions in minerals by the cryometric method. Geologiya i Geofizika 18, 16–27.

Crawford, M.L., 1981. Phase equilibria in aqueous fluid inclusions. In: Hollister, L.S., Crawford, M.L. (Eds.), Short course in fluid inclusions. Applications to Petrology. Mineralogical Association of Canada, 6, pp. 75–100.

Davis, D.W., Lowenstein, T.K., Spencer, R.J., 1990. Melting behaviour of fluid inclusions in laboratory-grown halite crystals in the system NaCl–H_2O, NaCl–KCl–H_2O, NaCl–$MgCl_2$–H_2O, NaCl–$CaCl_2$–H_2O. Geochimica et Cosmochimica Acta 54, 591–601.

Dubessy, J., Audeoud, D., Wilkins, R., Kosztolanyi, C., 1982. The use of the Raman microprobe Mole in the determination of the electrolytes dissolved in the aqueous phase of fluid inclusions. Chemical Geology 37, 137–150.

Dubessy, J., Boiron, M.C., Moissette, A., Monnin, C., Sretenskaya, N., 1992. Determinations of water, hydrates and pH in fluid inclusions by micro-Raman spectroscopy. European Journal of Mineralogy 4, 885–894.

Haynes, F.M., Sterner, M.S., Bodnar, R.J., 1988. Synthetic fluid inclusions in natural quartz. IV. Chemical analyses of fluid inclusions by SEM/EDA: evaluation of method. Geochimica et Cosmochimca Acta 52, 969–977.

Heinrich, C.H., Pettke, T., Halter, W.E., Aigner-Torres, M., Audètat, A., Günther, D., Hattendorf, B., Bleiner, D., Guillong, M., Horn, I., 2003. Quantitative multi-element analysis of minerals, fluid and melt inclusions by laser-ablation inductively-coupled-plasma mass-spectrometry. Geochimica et Cosmochimica Acta 67 (18), 3473–3496.

Kurosawa, M., Shimano, S., Ishii, S., Shima, K., Kato, T., 2003. Quantitative trace element analysis of single fluid inclusions by proton-induced X-ray emission (PIXE): application to fluid inclusions in hydrothermal quartz. Geochimica et Cosmochimica Acta 67 (22), 4337–4352.

Kwak, T.A.P., Hing Tan, T., 1981. The importance of $CaCl_2$ in fluid composition trends – evidence from the King Island (Dolphin) skarn deposit. Economic Geology 76 (4), 955–960.

Linke, W.F., 1958. Solubilities: Inorganic and metal-organic compounds, vol. I. American Chemical Society, Washington.

Ménez, B., Philippot, P., Bonnin-Mosbah, M., Simionovici, A., Gibert, F., 2002. Analysis of individual fluid inclusions using Synchotron X-ray Fluorescence microprobe: progress toward calibration for trace elements. Geochimica et Cosmochimica Acta 66 (4), 561–576.

Samson, I.M., Walker, R.T., 2000. Cryogenic Raman spectroscopic studies in the system NaCl–$CaCl_2$–H_2O and implications for low-temperature phase behaviour in aqueous fluid inclusions. The Canadian Mineralogist 38, 35–43.

Schiffries, C.M., 1990. Liquid-absent aqueous fluid inclusions and phase equilibria in the system $CaCl_2$–NaCl–H_2O. Geochimica et Cosmochimica Acta 54, 611–619.

Shephered, T.J., Rankin, A.H., Alderton, D.H.M., 1985. A Practical Guide to Fluid Inclusion Studies. Blackie & Son Ltd, Glasgow.

Vanko, D.A., Bodnar, R.J., Sterner, S.M., 1988. Synthetic fluid inclusions: VIII. Vapor-saturated halite solubility in part of the system NaCl–$CaCl_2$, with application to fluid inclusions from oceanic hydrothermal systems. Geochimica et Cosmochimica Acta 52, 2451–2456.

Yanatieva, C.K., 1946. Polythermal solubilities in the systems $CaCl_2$–$MgCl_2$–H_2O and $CaCl_2$–NaCl–H_2O. Zurnal prikladnoj chimii 19, 709–722 (in Russian).

Zwart, E.W., Touret, L.R., 1994. Melting behaviour and composition of aqueous fluid inclusions in fluorite and calcite: applications within the system H_2O–$CaCl_2$–NaCl. European Journal of Mineralogy 6, 773–786.